Heat-Dependent Hairpin Melting Drives Thermo-gated TRPV1 Opening

Guangyu Wang*

Department of Physiology and Membrane Biology, University of California School of Medicine, Davis, CA, USA

Department of Drug Research and Development, Institute of Biophysical Medico-chemistry, Reno, NV, USA

* Author to whom correspondence should be addressed; E-mail: gary.wang10@gmail.com

Abstract

The capsaicin receptor TRPV1 is a bio-thermometer in a primary afferent sensory neuron for noxious heat detection. However, the underlying molecular mechanism is unclear. Here, a hairpin thermodynamic model, together with graph theory, was to examine a role of temperature-dependent hairpin sizes in controlling the temperature threshold and sensitivity and gating states of TRPV1. The results showed that heat-dependent melting of the largest hairpin initiates a temperature threshold for channel opening while the smaller hairpins stabilize the open state and increase the heat efficacy or sensitivity. Therefore, this model may provide a broad structural basis for the thermo-gated TRP channels. (100 words)

Keywords: cooperative gating | desensitization | graph theory | hairpin thermodynamics | ion channel | non-covalent interaction | temperature sensitivity | threshold

1. INTRODUCTION

Temperature is important in everyday life. Transient receptor potential (TRP) vanilloid-1 (TRPV1) is well-known as a noxious heat sensor in a primary afferent neuron of the dorsal root and the trigeminal ganglia. Its activation allows sodium or calcium to be permeable to the channel pore. With a temperature activation threshold (~42°C) above a normal human body temperature 37°C and a temperature coefficient Q_{10} (defined as the ratio of equilibrium constants measured 10°C apart) higher than 20, this channel can work as a bio-thermometer to monitor any noxious heat signal and regulating the human body temperature. [1-4] In addition to the physical stimuli, capsaicin can also activate TRPV1, producing hot sensation. As cold can decrease the capsaicin-evoked activity of TRPV1, [5] the same gating pathway seems to be shared by both stimuli. On the other hand, residues sensitive to both physical and chemical stimuli are different in TRPV1, suggesting their different gating pathways. [6-9]

TRPV1 is a homotetramer with each monomer consisting of six transmembrane helices. The first four segments (S1–S4) form a voltage-sensor-like domain (VSLD) while the last two (S5 and S6), together with the intervening loop and the pore helix and the extracellular cap-like pore turret between S5 and S6, are folded as a pore domain. The pore domain is surrounded by the VSLD in a domain-swapped arrangement. The cation conductance pathway centers in the pore domain. A hydrophobic constriction around I697 forms a lower S6 gate while the segment from G643 to D646 (^{643}GMGD^{646}) between S5 and S6 (S5-P-S6) in rat TRPV1 (rTRPV1) acts as a short selectivity filter. The S4–S5 linker, which is a short amphipathic helix and almost parallel to the cytoplasmic membrane, couples the VSLD with the pore domain for channel gating. Thus, the overall structure of the TRPV1 channel resembles that of the voltage-gated ion channel. [10-11] However, TRPV1 has a conserved TRP domain, which runs parallel to the inner leaflet of the membrane by virtue of a sharp bend after S6, not only linking the S6 gate crossing bundle but also interacting with the S4–S5 linker and the pre-S1 domain in favor of allosteric coupling between different gating domains. In addition, the characteristic ankyrin repeats within the cytoplasmic N terminus can tether cytoplasmic N- and C-terminal domains for channel assembly. [11-14] Although the structural basis for the chemical stimuli such as capsaicin has been clear, [15-16] the heat-evoked gating pathway is still unknown for TRPV1 regarding the temperature threshold and sensitivity and desensitization.

Since 2013 a DNA hairpin thermal sensor with a 10-30 bases long poly-A loop has been created to monitor a change in a biological microenvironment. [17] Its hairpin melting curve is similar to the temperature-dependent gating of the thermosensitive TRPV channels. Its hairpin melting temperature are also in a threshold range of thermosensitive TRPV channels despite an increase with the smaller or less-flexible loop, the shorter duplexed stem, the more H-bonding pairs at the ends, or the higher ionic strength in an aqueous solution. [1, 6, 18-23] In this regard, it is fitting to ask if the thermosensitive TRPV channels exploit a series of hairpin topological structures to control the temperature thresholds and sensitivity or Q_{10} and gating states. In this study, graph theory was used as a novel method or tool to examine this hypothesis by analyzing the cryo-electron microscopy (cryo-EM) structural data of rTRPV1 with or without phosphatidylinositol (PI)-bound at the capsaicin site around the temperature threshold. The gating pathways of TRPV1 triggered by both physical and chemical stimuli were also compared and discussed.

2. RESULTS

2.1. The PI-free rTRPV1 Has Two Na^+ Cations in the Selectivity Filter to Generate the Largest Hairpin with a 32-residue Loop to Close the Channel at 4°C

When capsain competes off the PI lipid at low and high temperatures, this vanilloid compound does not bridge any residue in rTRPV1 to cause new hairpins under the given nanodisc condition. [14] Therefore, the state-dependent cryo-EM structures of PI-free rTRPV1 at different temperatures can be used as a group of controls to examine the role of temperature-dependent hairpin melting in the gating pathway.

At 4°C, several kinds of non-covalent interactions between amino acid side chains along the gating pathway from D388 in the pre-S1 domain to K710 in the TRP domain form a hairpin topological loop network to lock the PI-free rTRPV1 channel in the closed state.

First, salt bridges between charged pairwise residues are required to shape hairpins. They include E397-K710 and K425-E709 in the pre-S1/TRP interface, D471-R474 on S2, R499-D707 in the VSLD/TRP interface, D576-R579 on S5, E636-K639 on the pore helix, E684-K688 on S6 (Figure 1).

Second, π–π/cation interactions between aromatic side rings also bring about hairpins. In the VSLD and its interfaces with the pre-S1 domain and TRP domain and the S4-S5 linker, these π-interacting pairs cover W426-R701, F434-W426/Y555, F438-Y555/F559, Y441-

Y444/F488/F516/Y555, Y444-Y441/F448/F488, F488-Y441/Y444/F516, Y495-E513, F516-Y441/F488/N551/Y554, F522-F543, Y530-F531/Y537, and Y554-Y555. In the pore domain, the π-interacting pairs have F580-F584/L678, F589-T593, F591-Y666, Y627-F649, E636-F649, F640-Y666, and F659-Y653/F649 (Figure 1).

Third, H-bonds between different hydrophilic amino acid side chains also contribute the formation of hairpins. In the VSLD and the interfaces between the TRP domain and pre-S1 domain or the S4-S5 linker, these H-bonding pairs are Y401-D707, Q423-R701, Y441-Q519, T449-W549, Y487-R491, Q494-Q498, S505-D509, Q519-N551, and R557-Q700. In the pore domain and its interface with the TRP domain, the H-bonding pairs include D576-T685, Y584-T641/Y666, Q691-N695 (Figure 1).

Finally, the sulfurs from M644 in the selectivity filters and the hydroxyls from Y671 on S6 between two neighbor subunits bind two Na^+ cations in the permeation pathway to form the largest hairpin with a 32-residue loop consisting of Na^+-(M644-F649-F659-Y671)$_2$-Na^+ via inter-subunit metal bridges. Along the gating pathway from D388 to K710, the total numbers of all non-covalent interactions and hairpin sizes are 50 and 145, respectively (Figure 1).

2.2. The Removal of Na^+ Cations by Warm Temperature Releases the Dynamic Selectivity Filter

When the temperature raises from 4°C to 25°C, the inter-subunit metal bridges, M644-Na^+-M644 and Y671-Na^+-Y671, are broken so that the largest hairpin with a 32-residue loop melts and the dynamic selectivity filter is released. This metal removal does not open the channel but initiates several changes along the gating pathway. In the pore domain and its interfaces with the S4-S5 linker and the TRP domain, the new non-covalent interactions include the Y627-E636 and R575-T685 H-bonds and the K688-E692 salt bridge. In the S4-S5 linker/VSLD interface, the F438-F559 π–π interaction is disrupted with the new Q560-K694 and R557-T704 H-bonds in the S4-S5 linker/TRP interface. When the salt bridge shifts from R499-D707 to R491-D707 in the TRP/VSLD interface and D509 connects with R409 via a new salt bridge in the pre-S1/VSLD interface, the largest hairpin with a 21-residue loop is born from Y401 to R409, D509, S505, R491, D707 and back to Y401. As a result, the Y487-R491 and Q494-Q498 H-bonds are disconnected with the formation of the K466-D471 salt bridge. In addition, the CH-π interaction between Y495 and E513 is replaced with the F496-F517 π–π interaction. This global conformational change demonstrates that the pore domain is coupled to the VSLD via the interaction between the S4-S5

linker and the TRP domain. Along the gating pathway from D388 to K710, although the total number of all non-covalent interactions slightly increases from 50 to 52, the total number of all hairpin sizes significantly decreases from 145 to 132 (Figure 2).

2.3. The S2-S3 Linker and the Pre-S1 Domain and the TRP Domain Line the Largest Hairpin with a 21-residue Loop as a Heat Starter to Initiate a Temperature Threshold for Channel Opening above 25°C

When PI-free rTRPV1 opens at 48°C upon the melting of the largest hairpin with a 21-residues loop, several changes occur in non-covalent interactions. First, in the interfaces of the VSLD with the pre-S1 domain and the TRP domain, the R409-D509 and R491-D707 and E397-K710 and K425-E709 salt bridges and the Q423-R701 H-bond are broken. The H-bond also shifts from R557-T704 to Y554-T704. Second, in the interface of the VSLD with the S4-S5 linker, the π–π interaction shifts from Y555-F438 to F559-F434/F438 with the formation of the R557-E570 H-bond. When this conformational change extends to the VSLD, the D471-K466/R474 salt bridges, the S505-D509 and Q519-Y441/N551 H-bonds, and the Y441-F488 and Y530-F531 π–π interactions are disconnected. In the meanwhile, the Q494-Q498 H-bond is reinstated with formation of the new Y495-S510 H-bond and the new R499-D509 salt bridge. When this conformational change extends to the pore domain and its interfaces with the S4-S5 linker and the TRP domain, the Q560-K694 and R575-T685 and Y627-E636 and Q691-N695 H-bonds, the K688-E692 salt bridge, and the Y627-F649 π–π interaction are disrupted. Finally, the new T641-Y666 and D601-N628/N652 and N652-N628/T650 H-bonds are born with the shift of the salt bridge from E648-K656 to E651-K656. By all accounts, the total numbers of all non-covalent interactions and hairpin sizes along the gating pathway from D388 to K710 dramatically decrease from 52 and 134 to 44 add 85, respectively (Figure 3).

2.4. Smaller Hairpins in the Outer Pore and the S4-S5 Linker/S4 Interface Are Required to Stabilize the Open State and Related Heat Efficacy

In addition to the open state of PI-free rTRPV1 at 48°C, an intermediate state was also reported. [14] This state is different than the closed state at 25°C in the outer pore. For example, the Y627-E636 H-bond is disconnected with the formation of the Y653-K656 H-bond and the shift of the salt bridge from E648-K656 to E651-K656. On the other hand, this state is distinct from the open state at 48^0C in other domains and their interfaces. In the interfaces of the TRP domain with the pre-S1 domain and the VSLD and the S4-S5 linker and the pore domain, the Y401-D707

and Y554-T704 H-bonds are disrupted with the formation of the new E570-Q700 H-bond and the restoration of the Q691-N695 H-bond and the E397-K710 salt bridge. In the VSLD and its interface with the S4-S5 linker, the π–π interaction shifts from F434-F559 back to F434-Y555. When the Y441-F488 π–π interaction is reinstated with the presence of the Q519-Y441/Y444/N551 H-bonds, the Y495-S510 H-bond and the R499-D509 salt bridge and the F496-F517 π–π interaction are replaced with the R491-Q494 and Y495-R499 H-bonds. As a result, several smallest hairpins with no residue in the loops appear among triple residues. For example, R557-E570-Q700 in the S4-S5 linker/TRP interface, Q519-Y441-Y444 and Y441-Y444-F488, F488-F516-Y441 in the VSLD. Taken together, although the total number of all non-covalent interactions along the gating pathway from D388 to K710 is still around 44, the total number of all the hairpin sizes significantly decreases from 85 to 68 residues (Figure 4). In other words, this so-called intermediate is much more stable than the open state and thus serves as an inactivated state. In that regard, three smaller hairpins are required to stabilize the open state and the related heat efficacy. The first has 12 residues in the loop from R557 to E570 linking the VSLD with the critical S4-S5 linker to prime the opening of the lower gate. The second has no residue in the loop from D601 to N628 and N652. The third has no residue in the loop formed by the Y584-T641-Y666 H-bonding triangle network (Figures 2-4).

2.5. The largest Hairpin with a 17-residue Loop Prevents the PI-bound rTRPV1 from Opening at 48°C under the Given Nanodisc Condition

When the resident PI occupies the well-known vanilloid site, rTRPV1 cannot open even at 48°C when reconstituted into lipid nanodiscs. This closed state of PI-bound rTRPV1 is almost identical between 4°C and 48°C. [14] However, compared to PI-free rTRPV1 at 25°C, there are several differences. First, the PI lipid links D509, N551, R557, E570 and Q700 together via H-bonds. As a result, in the pore domain and its interfaces with the S4-S5 linker and the TRP domain, the E648-K656 and K688-E692 salt bridges and the R575-T685 H-bond are disrupted with the formation of the E692-K571/R575 salt bridges. In the VSLD, the K466-D471 salt bridge and the S505-D509 H-bond are disrupted with the formation of the Y487-R491 H-bond, and the shift of the π interaction from F496-F517 to Y495-E513. More importantly, when the R557-T704 H-bond is broken and the salt bridge shifts from R491-D707 to R499-D707 in the VSLD/TRP interface, the largest hairpin decreases the size from 21 to 17 residues in the loop. It starts with R499 and through D707 and Y401 and R409 and ends with D509 (Figure 5).

3. DISCUSSION

TRPV1 is designed and created as a template of bio-thermometers in the thermostable system to detect noxious heat and to protect an animal body from heat damage. [1-4] To this end, it should meet several protein engineering requirements. First, it should be an integral membrane protein with a relative high physicochemical stability or heat capacity to avoid thermal denaturation. Second, it should be an ion channel to directly couple a temperature signal to an electronical signal reporter for a readout by a primary afferent sensory neuron. Third, its opening from the closed state should have a high Q_{10} with a steep response to a small change in a surround predetermined temperature. Fourth, it should have an inactivated state to be responsible for use-dependent desensitization to alleviate pain upon constant noxious heat stimuli. In the biological and chemical world, a hairpin topological loop structure may be an ideal tool for thermosensitive TRP channels to control such a high Q_{10} and a variety of temperature thresholds and gating states.

The DNA hairpin with limited loop sizes has been designed as a temperature switch, a thermometer and an ionic detector with Q_{10} in the range from 1.7 to 4. Its oligonucleotides with complementary nucleotide sequences at the ends form a duplex region as the hairpin stem upon intra-strand hybridization, and its nucleotides in between as the hairpin loop. When a temperature increases above a threshold, the DNA hairpin will melt and thus becomes single stranded. Its melting temperature sharply depends on the H-bonded base pairs in the stem, the size and flexibility of the loop and the ionic strength in a solution. Generally, a stable stem or a small and rigid loop or a high salt concentration in the solution allow the DNA hairpin to have a high threshold to sense and to respond to highly specific and small changes in an environmental temperature. When the loop length is decreased from 20 to 10 A's or the H-bonded G-C base-pairs raise from 2 to 4, the melting temperature can be increased more than 20 degrees. Clearly, a short stem favors sharp hairpin melting rather than gradual melting. Since a change in the loop sequence has no significant effect on the melting temperature of the DNA biosensor, [17] once noncovalent interactions create a hairpin topological loop, the hairpin thermodynamics should be comparable between DNA and protein.

Like the DNA hairpin thermal biosensor, when three to four non-covalent interactions make the largest hairpin along the gating pathway from D388 in the pre-S1 domain to K710 in TRPV1 in the physiological salt concentration range (150 mM NaCl), the melting temperature increases

with the decreased size. The presence of two inter-subunit metal bridges, M644-Na^+-M644 and Y671-Na^+-Y671, together with the F649-F659 π–π interactions in PI-free rTRPV1, produces the first largest hairpin with a 32-residue loop Na^+-(M644-F649-F659-Y671)$_2$-Na^+ in the pore domain at 4°C (Figure 1). Its melting at 25°C induces the formation of the second largest hairpin with a 21-residue loop from Y401 to R409, D509, S505, R491 and D707 via the Y401-D707 and S505-D509 H-bonds and the R409-D509 and R491-D707 salt bridges (Figure 2). The melting of the second one at 48°C further decreases the size of the largest hairpin to 10-13 residues in the loops (Figures 3-4). In stark contrast, the largest hairpin with a 17-residue loop without the S505-D509 H-bond in the same interfaces of the VSLD and the TRP domain and the pre-S1 domain cannot melt at 48°C to allow PI-bound rTRPV1 to open under the given nanodisc condition (Figure 5). Therefore, the hairpin thermodynamics between DNA and protein is equivalent once non-covalent interactions create a hairpin topological loop.

Although the first and second largest hairpins with 32 and 21 residues in the loops of rTRPV1 melt at 25°C and 48°C, respectively (Figures 1-4), they have distinct gating effects. The melting of the first one releases Na^+ from the selectivity filter but does not significantly change the non-covalent interactions and the related hairpin topological structure in the pore domain. Thus, the PI-free rTRPV1 is still closed. By contrast, the second one is coupled to the lower S6 gate. Its melting disrupts the interactions of the S2-S3 linker with the TRP domain and the pre-S1 domain, allowing PI-free rTRPV1 to open (Figure 6). This result is consistent with the notion that the channel gating is governed by inter-domain interactions. Further experiments are necessary to examine the role of the Y401-D707 and S505-D509 H-bonds and the R409-D509 and R491-D707 salt bridges in initiating the temperature threshold for rTRPV1 opening. Since R409 and D509 in rTRPV1 are also conserved in thermosensitive TRPV2-4 but not in non-thermosensitive TRPV5-6, [24] it is attractive to test if the R409-D509 salt bridge in rTRPV1 is also conserved in TRPV2-4 for the relevant largest hairpin to be responsible for the temperature threshold.

In addition the largest hairpin to be responsible for the primary temperature threshold of TRPV1, other smaller hairpins play a critical role in not only regulating the temperature threshold and gating states and related heat efficacy or sensitivity but also stopping heat denaturation (Figure 6).

The first has no residue in the loop from Y441 and though F516 and Y554 and Y555 and back to Y441. This smallest hairpin is shared by both closed and open states (Figures 2-3), and

the related aromatic residues are highly conserved in thermosensitive TRPV1-4 but not in non-thermosensitive TRPV5-6. [24] The tight π interactions allow this smallest hairpin to serve as a relatively stationary anchor against which the S4–S5 linker can uplift in favor of TRPV1 opening. In support of this notion, the Y441S, Y444S, Y554A or Y555S mutation leaves the channel not functional. [25-26]

The second has 12 residues in the loop from R557 to E570 as shown in the open state of the TRPV1 only (Figures 3, 6). As the mutation R557E/A/L or E570L/A can disrupt the stimulatory R557-E570 salt bridge or H-bond, it is reasonable that the R557E or E570L mutant leads to a complete loss of function, mutants R557A/L and E570A have low heat sensitivity, and E570A increases the threshold from 41.5°C to 44.3°C. [25, 27] Of special note, when R557 and E570 and Q700 form an H-bond triangle for the smallest hairpin to have no residue in the loop, the total hairpin sizes along the gating pathway from D388 to K710 are much less in the so-called intermediate than in the open state (Figures 3-4). Therefore, the reported intermediate is more likely than not to be an inactivated state for use-dependent desensitization in response to the constant heat stimuli. [1, 8, 14, 28]

The third has a 7-residue loop from D576 to K579 and F580 and L678 and T685 via the D576-T685 H-bond and the D576-R579 salt bridge and the F580-L678 CH-π interaction. It has been reported that the mutant R579E is not functional and the D576N/R or R579A mutant is less sensitive to heat than wild type rTRPV1. [25] Since the residues for this smaller hairpin are conserved in TRPV1-6, it may serves a key anchor in the pore domain. [24]

The fourth has no residue in the loop from Y584 to T641 and F640 and Y666 and back to Y584. The residues for this smallest hairpin are also highly conserved in TRPV1-4 but not in TRPV5-6. [24] In agreement with its importance, the Y666A mutation is not functional while the F640L or T641S mutation decreases the temperature threshold to allow those two mutants to be constitutively active at room temperature. [29-30]

The fifth has no residue in the loop once formed by the N628-D601-N652 H-bonding triangle. It has been reported that the N628K or N652T or Y653T or combined mutation increases the temperature threshold, and the triple mutant N628K/N652T/Y653T has the longer opening durations [7] Furthermore, the N628L greatly decreases the heat sensitivity but the N628D has the opposite effect, [14] possibly by mediating the heat stablity of this smallest hairpin.

Notebly, the turret deletion or replacement with glycine between G603 and N626 in mouse TRPV1 (mTRPV1) decreases the temperature threshold to a different extent, [8] possibly because these manipulations may induce the formation of the new largest hairpin with a size larger than 21 residues in the loop along the gating pathway from D388 to K710. More importantly, although the deletion of the turret (Δ604-626) still allows the TRPV1 mutant construct to be activated by heat, the binding of external double-knot toxin or vanillotoxin (DkTX) to the outer pore prevents heat activation, possibly by disrupting the hairpin-forming N628-D601-N652 and Y584-T7641-Y666 H-bonding network [9, 15]

Previous study of a cyclic β-hairpin peptide of the general sequence XRTVXVdPGOXITQX demonstrated that although a hydrophobic cluster is typically necessary for stabilizing a β-hairpin, [31-32] the aromatic residues stabilize the hairpin more than the salt bridges at a non-hydrogen-bonded internal and terminal position. The aromatic pairs enthalpically prefer a favorable edge-face π–π attractive interaction, whereas the folding of hairpins with cross-strand salt bridge is more entropically favorable than enthalpically favorable. Thus, aromatic π–π attractive interactions play a pivotal role in forming a tightly-folded hairpin and thus increasing enthalpy and decreasing entropy. [33]

In the case of heat-activated TRPV1, the opening of multiple larger hairpins increases entropy as a result of the disruption of most of the salt bridges along the gating pathway from D388 to K710 (Figures 2-3). However, the dramatic decrease in the total number of all hairpin sizes from 132 in the closed state to 85 in the open state may increase enthalpy to secure the larger heat capacity. Thus, a small decrease in the free energy is enough for intra-molecular gating rearrangements to activate TRPV1 with the higher temperature sensitivity and to meet its protein engineering requirement for noxious heat detection. On the other hand, the short hairpin stem with a non-covalent interaction, together with the coupled gating rearrangements of hairpins along the gating pathway in a physiological salt concentration range, may allow the product of multiple related smaller Q_{10} values upon hairpin opening and closure to be responsible for the high thermal sensitivity or the large Q_{10}. Alternatively and simply, $Q_{10} \approx (132-85)/2 = 23.5$ (Figures 2-3, 6).

When the resident PI lipid in the capsaicin pocket links D509, N551, R557, E570 and Q700 together via H-bonds, this PI binding in the primary closed state does not change the largest hairpin size in the interfaces of the VSLD with the TRP domain and the pre-S1 domain (Figure 5). Thus, the temperature threshold seems to be independent of the PI lipid. However, the release of the PI

lipid from the vanilloid site facilitates the formation of the stimulatory R557-E570 H-bond to stabilize the heat efficacy (Figures 2-3). Therefore, the PI release from the capsaicin site may be required for heat activation.

Although both capsaicin and heat can activate rTRPV1 eliciting hot sensation, they are different in two aspects. First, capsaicin potency and efficacy are based on the same binding site above the S4-S5 linker and between S3/S4 and S5/S6. The vanilloid bridge via the H-bond between the side chains of T551 on S4 and E570 in the S4-S5 linker can prime the capsaicin affinity and efficacy by uplifting the S4-S5 linker. [15-16] However, the heat threshold and efficacy in PI-free rTRPV1 may be separated. The largest hairpin with a 21-residue loop from Y401 to R409, D509, S505, R491, D707 and back to Y401 in the interface between the VSLD and the TRP domain or the pre-S1 domain may be responsible for the heat threshold 42°C. On the other hand, the R557-E570 H-bond in the S4-S5 linker/VSLD interface, together with the N652-D601-N628 and Y584-T641-Y666 H-bond networks in the outer pore, may be needed to stabilize open state and the related heat efficacy (Figures 2-3). [14] Second, capsaicin competes off the resident lipid via the anchor-stereoselective vanilloid bridge in the capsaicin pocket. [16] In contrast, heat may open the largest hairpin loop around the resident PI lipid to release it from the capsaicin site if necessary for channel opening.

The prior study suggested that F435 on S1, F516 on S3, Y545 and Y555 and R557 may form a putative menthol pocket in human TRPV1 (hTRPV1). [34] Since menthol only partly stop the heat activation of TRPV1 without changing the temperature threshold, [35-36] this putative menthol site may not alter the largest hairpin with a 21-residue loop in the VSLD/TRP/pre-S1/VSLD interfaces but may weaken the heat-sensitive R557-E570 H-bond. [25, 27]

Other chemical stimuli have been reported to lower the temperature threshold of mTRPV1 to a different extent in a dose-dependent manner. For example, external Mg^{2+} binding to possible residues such as N652 and D601 and N628 in the outer pore or intracellular niacin binding to putative residues S512 and R557 and E570 in the VSLD/S4-S5 linker interface. [37-39] These two chemical stimuli may allosterically weaken the R409-D509 or R491-D707 salt bridge or the Y401-F707 H-bond that is required to form the largest hairpin with a 21-residue loop as the basis for the normal threshold 42°C.

Inter-domain non-covalent interactions have been reported to regulate the gating pathway of ion channels at room temperatures. [16, 34, 40-48] Here, this study further demonstrates that the

largest and smaller hairpins along the gating pathway play critical roles in regulating a series of biochemical reaction networks to initiate a temperature threshold and to stabilize the thermal activity of the heat-sensing TRPV1 channel, respectively. Further investigation is necessary to extend to other thermosensitive TRP channels.

4. CLOSING REMARK

The hairpin topological loop structures can be used to design a thermosensitive biological thermometer with a high Q_{10} value. In addition to the ionic strength in the physiological range, the hairpin size and the number and the intensity of the hairpin-forming non-covalent interactions between amino acid side chains can be used to tune different melting temperatures as thresholds for the detection of distinct small environmental temperature changes. They include salt bridges, aromatic side chain π interactions, H-bonds and metal bridges. Both the largest and smaller hairpins are necessary to control the temperature threshold and the thermal efficacy. Their opening and closure should be reversible and fast enough to have a very large effect on channel gating, which can be easily coupled to an electrical readout in the primary afferent sensor neuron. In this regard, this study may provide a broad structural basis for thermosensitive TRP channels to work as a bio-thermometer.

5. MATERIALS AND METHODS

In this *in silicon* study, the hairpin topological structural aspects of rTRPV1 channels below and above the temperature threshold were investigated and analyzed with graph theory, a novel method and tool, as the thermometer basis for noxious heat detection. The *in silicon* protomer models were based on the cryo-EM structural data of closed rTRPV1 in MSP2N2 with PI-bound at 4°C (PDB ID, 7LP9, model resolution= 2.63 Å) and 48°C (PDB ID, 7LPC, model resolution= 3.07 Å), capsaicin-bound at 4°C (PDB ID, 7LPA, model resolution= 3.37 Å) and 25°C (PDB ID, 7LPB, model resolution= 3.54 Å) and 48°C (PDB ID, 7LPD, model resolution= 3.55 Å), open rTRPV1 with capsaicin-bound at 48°C (PDB ID, 7LPE, model resolution= 3.72 Å), [14] UCSF Chimera was used to assess the presence of non-covalent interactions in TRPV1. All the stereo- or regioselective diagonal and lateral non-covalent interactions such as salt-bridges and lone pair/CH/cation-π interactions and H-bonds and metal bridges between amino acid side chains along the gating pathway from D388 in the pre-S1 domain to K710 in he TRP domain of rTRPV1

were included to test their potential roles in forming the minimum hairpin sizes, controlling the temperature threshold and stablizing the heat afficacy for the higher temperature coefficient Q_{10}. The standard definition of noncovalent interactions was employed.

The minimum hairpin sizes to control the intensity of non-covalent interactrions were calculated using graph theory. The primary amino acid sequence line from D388 to K710 was marked in black. An amino acid side chain involving a non-covalent interaction along the gating pathway of rTRPV1 was defined as a vertex and marked with an arrow in different colors. The same kind of non-covalent interactions between two amino acid side chains was marked with an edge in the same color. A hairpin topologicval loop was considered significant when an edge forms a sealed topological ring with the amino acid sequence between two ends of the edge or other edges. If n was the sum of the sequence number differences between two adjacent vertexes in a hairpin topologcal loop, the loop size was defined as (n-1). The minimum hairpin topological loop to control the thermostability of a non-covalent interactrion was definded with the least product of the number of non-covalent interactions in the loop and the loop size. Only the minimum hairpin topological loop sizes were marked in black. The largest or gating hairpin sizes were shown in a red circle. The total number of all noncovalent interactions and hairpin sizes along the gating pathway were shown in black and blue circles, respectively.

Q_{10} was used to characterize the temperature-dependent responses as calculated using the following equation:

$$Q_{10} = (R2/R1)^{10/(T2-T1)}$$

where, R1 and R2 are rates of a reaction at two different temperatures T1 and T2 in Celsius degrees or kelvin, respectively.

Conventions and Abbreviations: cryo-EM, cryo-electron microscopy; DkTx, double-knot toxin or vanillotoxin; PI, phosphatidylinositol; TRP, transient receptor potential; TRPV1, TRP vanilloid-1; TRPVi (i=1; 2, 3, 4, 5, 6); hTRPV1, human TRPV1; mTRPV1, mouse TRPV1; rTRPV1, rat TRPV1; VSLD, voltage-sensor-like domain

Acknowledgements

The author's own studies cited in this article were supported by NIDDK Grant (DK45880 to D.C.D.) and Cystic Fibrosis Foundation grant (DAWSON0210) and NIDDK grant (2R56DK056796-10) and American Heart Association (AHA) Grant (10SDG4120011 to GW).

Conflict of Interest: The author declares no conflict of interest.

Data Availability Section: This study includes no data deposited in external repositories

References

1. M. J. Caterina, M. A. Schumacher, M. Tominaga, T. A. Rosen, J. D. Levine, D. Julius. The capsaicin receptor: a heat-activated ion channel in the pain pathway. *Nature* **1997**, 389, 816.
2. J. B. Davis, J. Gray, M. J. Gunthorpe, J. P. Hatcher, P. T. Davey, P. Overend, M. H. Harries, J. Latcham, C. Clapham, K. Atkinson, S. A. Hughes, K. Rance, E. Grau, A. J. Harper, P. L. Pugh, D. C. Rogers, S. Bingham, A. Randall, S. A. Sheardown. Vanilloid receptor-1 is essential for inflammatory thermal hyperalgesia. *Nature* **2000**, 405,183.
3. N. R Gavva; J. J. S. Treanor, A. Garami, L. Fang, S. Surapaneni, A. Akrami, F. Alvarez, A. Bak, M. Darling, A. Gore, G. R. Jang, J. P. Kesslak, L.Ni, M. H. Norman, G. Palluconi, M. J. Rose, M. Salfi, E. Tan, A. A. Romanovsky, C. Banfield, G. Davar. Pharmacological blockade of the vanilloid receptor TRPV1 elicits marked hyperthermia in humans. *Pain* **2008**, 136, 202.
4. I. Vandewauw, K. De Clercq, M. Mulier, K. Held, S. Pinto, N. V. Ranst, A. Segal, T. Voet, R. Vennekens, K. Zimmermann, J. Vriens, T. Voets. A TRP channel trio mediates acute noxious heat sensing. *Nature* **2018**, 555, 662.
5. M. K. Chung, S. Wang. Cold suppresses agonist-induced activation of TRPV1. *J Dent Res* **2011**, 90, 1098.
6. S. E. Jordt, D. Julius. Molecular basis for species-specific sensitivity to “hot” chili peppers. *Cell* **2002**, 108, 421.
7. J. Grandl, S. E. Kim, V. Uzzell, B. Bursulaya, M. Petrus, M. Bandell, A. Patapoutian. Temperature-induced opening of TRPV1 ion channel is stabilized by the pore domain. *Nat Neurosci.* **2010**, 13, 708.
8. Y. Cui, F. Yang, X. Cao, V. Y. Yarovoy, K.W. Wang, J. Zheng. Selective disruption of high sensitivity heat activation but not capsaicin activation of TRPV1 channels by pore turret mutations. *J. Gen. Physiol.* **2012**, 139, 273.
9. A. Jara-Oseguera, C. Bae, K. J. Swartz. An external sodium ion binding site controls allosteric gating in TRPV1 channels. *Elife* **2016**, 5.
10. S. B. Long, E. B. Campbell, R. Mackinnon. Crystal structure of a mammalian voltage-dependent Shaker family K^+ channel. *Science* **2005**, 309, 897.

11. M. Liao, E. Cao, D. Julius, Y. Cheng. Structure of the TRPV1 ion channel determined by electron cryo-microscopy. *Nature* **2013**, 504,107.
12. E. Cao, M. Liao, Y. Cheng, D. Julius. TRPV1 structures in distinct conformations reveal activation mechanisms. *Nature* **2003**, 504, 113.
13. K. D. Nadezhdin, A. Neuberger, Y. A. Nikolaev, L. A. Murphy, E. O. Gracheva, S. N. Bagriantsev, A. I. Sobolevsky. Extracellular cap domain is an essential component of the TRPV1 gating mechanism. *Nat Commun.* **2021**, 12, 2154.
14. D. H. Kwon, F. Zhang, Y. Suo, J. Bouvette, M. J. Borgnia, S.-Y. Lee, Heat-dependent opening of TRPV1 in the presence of capsaicin. *Nat Struct Mol Biol*. **2021**, 28, 554.
15. Y. Gao, E. Cao, D. Julius, Y. Cheng. TRPV1 structures in nanodiscs reveal mechanisms of ligand and lipid action. *Nature* **2016**, 534, 347.
16. G. Wang. Lipid-dependent sequential allosteric activation of heat-sensing TRPV1 channels by anchor-stereoselective "hot" vanilloid compounds and analogs. *Biochem. Biophys. Rep*. **2000**, 28, 101109.
17. A. T. Jonstrup, J. Fredsøe, A. H. Andersen. DNA Hairpins as Temperature Switches, Thermometers and Ionic Detectors. *Sensors* **2013**, 13, 5937.
18. M. J. Caterina, T. A. Rosen, M. Tominaga, A. J Brake, D. Julius. A capsaicin-receptor homologue with a high threshold for noxious heat. *Nature* **1999**, 398,436.
19. M. J. Caterina, A. Leffler, A. B. Malmberg, W. J. Martin, J. Trafton, K. R. Petersen-Zeitz, M. Koltzenburg, A. I. Basbaum, D. Julius. Impaired nociception and pain sensation in mice lacking the capsaicin receptor. *Science* **2000**, 288, 306.
20. A. M. Peier, A. J. Reeve, D. A. Andersson, A. Moqrich, T. J. Earley, A. C. Hergarden, G. M. Story, S. Colley, J. B. Hogenesch, P. McIntyre, S. Bevan, A. Patapoutian. A heat-sensitive TRP channel expressed in keratinocytes. *Science*. **2002,** 296, 2046.
21. G. D. Smith, M. J. Gunthorpe, R. E. Kelsell, P. D. Hayes, P. Reilly, P. Facer, J. E. Wright, J. C. Jerman, J-P. Walhin, L. Ooi, J. Egerton, K. J. Charles, D. Smart, A. D. Randall, P. Anand, J. B. Davis. TRPV3 is a temperature-sensitive vanilloid receptor-like protein. *Nature* **2002**, 418, 186.
22. H. Xu, I. S. Ramsey, S. A. Kotecha, M. M. Moran, J. A. Chong, D. Lawson, P. Ge, J. Lilly, I. Silos-Santiago, Y. Xie, P. S. DiStefano, R. Curtis, D. E. Clapham. TRPV3 is a calcium-permeable temperature-sensitive cation channel. *Nature* **2002**, 418, 181.

23. M. K. Chung, H. Lee, M. J. Caterina. Warm temperatures activate TRPV4 in mouse 308 keratinocytes. *J. Biol. Chem*. **2003**, 278, 32037.
24. K. D. Nadezhdin, A. Neuberger, Y. A. Trofimov , N. A. Krylov , V. Sinica, , N. Kupko, V. Vlachova , E. Zakharian , R. G. Efremov, A. I. Sobo-levsky. Structural mechanism of heat-induced opening of a temperature-sensitive TRP channel. *Nat. Struct. Mol. Biol.* **2021,** 28, 564–572.
25. S. Boukalova, L. Marsakova, J. Teisinger, V. Vlachova. Conserved residues within the putative S4–S5 region serve distinct functions among thermosensitive vanilloid transient receptor potential (TRPV) channels. *J. Biol. Chem*. **2010**, 285, 41455.
26. Boukalova, S., Teisinger, J. &Vlachova,V. Protons stabilize the closed conformation of gain-of-function mutants of the TRPV1 channel. *Biochim. Biophys. Acta*. **2013,** 1833,520.
27. M. Kim, N. J. Sisco, J. K. Hilton, C. M. Montano, M. A. Castro, B. R. Cherry, M. Levitus, W. D. V. Horn. Evidence that the TRPV1 S1-S4 membrane domain contributes to thermosensing. *Nat Commun.* **2020**, 11, 4169.
28. L. Luo, Y. Wang, B. Li, L. Xu, P. M. Kamau, J. Zheng, F. Yang, S. Yang, R. Lai. Molecular basis for heat desensitization of TRPV1 ion channels. *Nat Commun.* **2019,** 10, 2134. Correction in: *Nat Commun*. **2020;** 11, 1798.
29. K. Susankova, R. Ettrich, L. Vyklicky, J. Teisinger, V. Vlachova. Contribution of the Putative Inner-Pore Region to the Gating of the Transient Receptor Potential Vanilloid Subtype1 Channel (TRPV1). *J. Neurosci.* **2007,** 27, 7578.
30. B. R. Myers, C. J. Bohlen, D. Julius. A yeast genetic screen reveals a critical role for the pore helix domain in TRP channel gating. *Neuron* **2008**, 58, 362.
31. A. J. Maynard, G. J. Sharman, M. S. Searle. Origin of β-hairpin stability in solution: Structural and thermodynamic analysis of the folding of model peptide supports hydrophobic stabilization in water. *J. Am. Chem. Soc*. **1998**, 120, 1996.
32. J. F. Espinosa, S. H. Gellman. A designed β-hairpin containing a natural hydrophobic cluster. *Angew Chem. Int. Edit*. **2000**, 39, 2330.
33. S. E. Kiehna, M. L. Waters. Sequence dependence of β-hairpin structure: Comparison of a salt bridge and an aromatic interaction. *Protein Science* **2003**, 12, 2657.

34. G Wang. Ligand-stereoselective allosteric activation of cold-sensing TRPM8 channels by an H-bonded homochiral menthol dimer with head-to-head or head-to-tail. *Chirality* **2021**, 33, 783.
35. M Takaishi, K. Uchida, Y. Suzuki, H. Matsui, T. Shimada, F. Fujita, M. Tominaga. Reciprocal effects of capsaicin and menthol on thermosensation through regulated activities of TRPV1 and TRPM8. *J Physiol Sci.* **2016**, 66, 143.
36. T. H. D Nguyen, S. G. Itoh, H. Okumura, M. Tominaga. Structural basis for promiscuous action of monoterpenes on TRP channels. *Commun Biol*. **2021**, 4, 293.
37. X. Cao, L. Ma, F. Yang, K. W. Wang, J. Zheng. Divalent cations potentiate TRPV1 channel by lowering the heat activation threshold. *J Gen Physiol*. **2014**, 143, 75.
38. L. Ma, B. H. Lee, R. Mao, A. Cai, Y. Jia, H. Clifton, S. Schaefer, L. Xu, J. Zheng. Nicotinic Acid Activates the Capsaicin Receptor TRPV1 Potential Mechanism for Cutaneous Flushing. *Arterioscler Thromb Vasc Biol*. **2014**, 34, 1272.
39. L. Ma, B. H. Lee, H. Clifton, S. Schaefer, J. Zheng. Nicotinic Acid is a Common Regulator of Heat-Sensing TRPV1-4 Ion Channels. *Sci. Rep***. 2015**, 5, 8906.
40. G Wang. State-dependent regulation of cystic fibrosis transmembrane conductance regulator (CFTR) gating by a high affinity Fe^{3+} bridge between the regulatory domain and cytoplasmic loop 3. *J Biol Chem* **2010**, 285, 40438.
41. W. Wang, J. Wu, K. Bernard, G. Li, G. Wang, W. Bevensee, K. L. Kirk. ATP-independent CFTR channel gating and allosteric modulation by phosphorylation. *Proc Natl Acad Sci USA*, **2010**, 107, 3888.
42. G. Wang. The inhibition mechanism of non-phosphorylated Ser768 in the regulatory domain of cystic fibrosis transmembrane conductance regulator. *J Biol Chem*. **2011**, 286, 2171.
43. G. Wang, D. D. Duan. Regulation of activation and processing of the cystic fibrosis transmembrane conductance regulator (CFTR) by a complex electrostatic interaction between the regulatory domain and cytoplasmic Loop 3. *J Biol Chem* **2012**, 287, 40484.
44. G. Wang. Interplay between inhibitory ferric and stimulatory curcumin regulates phosphorylation-dependent human cystic fibrosis transmembrane conductance regulator and ΔF508 activity. *Biochemistry* **2015**, 54, 1558.

45. G. Wang. Molecular Basis for Fe(III)-Independent Curcumin Potentiation of Cystic Fibrosis Transmembrane Conductance Regulator Activity. *Biochemistry* **2015**, 54, 2828.
46. G. Wang, R. Linsley, Y. Norimatsu. External Zn^{2+} binding to cysteine-substituted cystic fibrosis transmembrane conductance regulator constructs regulates channel gating and curcumin potentiation. *FEBS J* **2016**, 283, 2458.
47. G. Wang. Mechanistic insight into the heme-independent interplay between iron and cartbon monoxide in CFTR and *Slo1* BKca channels. *Metallomics* **2017**, 9, 634.
48. G. Wang. Removal of the Fe(III) site promotes activation of the human cystic fibrosis transmembrane conductance regulator by high-affinity Zn(II) binding. *Metallomics* **2018**, 10, 240.

Figure legends

Figure 1. **The hairpin topological structures along the gating pathway of PI-free rTRPV1 in the closed state at 4°C. A,** Pairing amino acids side chains for salt bridges or H-bonds or lone pair/cation/CH/π-π interactions along the gating pathway from D388 to K710. The cryo-EM structure of closed rTRPV1 with capsaicin bound at 4°C (PDB ID, 7LPA) was used for the model.[14] The residues are colored in red for a positive charge or blue for a negative charge or orange for the uncharged residues in salt bridges or H-bonds or lone pair/cation/CH/π-π interactions, and green for π interactions. The largest hairpin with a 32-residue loop in the interface between two pore domains is shown in the right panel. **B**, The hairpin topological loop map of PI-free rTRPV1 in the closed state at 4°C. The pore domain, the S4-S5 linker, the TRP domain, the VSLD and the pre-S1 domain are indicated in black. Salt bridges, π interactions, and H-bonds between amino acid side chains along the gating pathway from D388 to K710 are marked in purple, green, and orange, respectively. The minimum hairpin topological loop sizes required to control the relevant non-covalent interactions are labeled in black. The total numbers of all hairpin loop sizes and non-covalent interactions along the gating pathway are shown in the blue and black circles, respectively.

Figure 2. **The hairpin topological structures along the gating pathway of PI-free rTRPV1 in the closed state at 25°C. A,** Pairing amino acids side chains for salt bridges or H-bonds or lone pair/cation/CH/π-π interactions along the gating pathway from D388 to K710. The cryo-EM structure of closed rTRPV1 with capsaicin bound at 25°C (PDB ID, 7LPB) was used for the model.[14] The residues are colored in red for a positive charge or blue for a negative charge or orange for the uncharged residues in salt bridges or H-bonds or lone pair/cation/CH/π-π interactions, and green for π interactions. The largest hairpin with a 21-residue loop in the interfaces of the VSLD with the TRP domain and the pre-S1 doamin is shown in the right panel. **B**, The hairpin topological loop map of PI-free rTRPV1 in the closed state at 25°C. The pore domain, the S4-S5 linker, the TRP domain, the VSLD and the pre-S1 domain are indicated in black. Salt bridges, π interactions, and H-bonds between amino acid side chains along the gating pathway from D388 to K710 are marked in purple, green, and orange, respectively. The minimum hairpin topological loop sizes required to control the relevant non-covalent interactions are labeled in black.

The total numbers of all hairpin loop sizes and non-covalent interactions along the gating pathway are shown in the blue and black circles, respectively.

Figure 3. **The hairpin topological structures along the gating pathway of PI-free rTRPV1 in the open state at 48°C. A,** Pairing amino acids side chains for salt bridges or H-bonds or cation/CH/π-π interactions along the gating pathway from D388 to K710. The cryo-EM structure of open rTRPV1 with capsaicin bound at 48°C (PDB ID, 7LPE) was used for the model. [14] The residues are colored in red for a positive charge or blue for a negative charge or orange for the uncharged residues in salt bridges or H-bonds or cation/CH/π-π interactions, and slight green for π interactions. The largest hairpin with a 13-residue loop in the S2-S3 linker is shown in the right panel. **B**, The hairpin topological loop map of PI-free rTRPV1 in the open state at 48°C. The pore domain, the S4-S5 linker, the TRP domain, the VSLD and the pre-S1 domain are indicated in black. Salt bridges, π interactions, and H-bonds between amino acid side chains along the gating pathway from D388 to K710 are marked in purple, green, and orange, respectively. The minimum hairpin topological loop sizes required to control the relevant non-covalent interactions are labeled in black. The total numbers of all hairpin loop sizes and non-covalent interactions along the gating pathway are shown in the blue and black circles, respectively.

Figure 4. **The hairpin topological structures along the gating pathway of PI-free rTRPV1 in the desensitized state at 48°C. A,** Pairing amino acids side chains for salt bridges or H-bonds or cation/CH/π-π interactions along the gating pathway from D388 to K710. The cryo-EM structure of inactivated rTRPV1 with capsaicin bound at 48°C (PDB ID, 7LPD) was used for the model.[14] The residues are colored in red for a positive charge or blue for a negative charge or orange for the uncharged residues in salt bridges or H-bonds or cation/CH/π-π interactions, and slight green for π interactions. The largest hairpin with a 10-residue loop in the S2-S3 interface is shown in the right panel. **B**, The hairpin topological loop map of PI-free rTRPV1 in the desensitized state at 48°C. The pore domain, the S4-S5 linker, the TRP domain, the VSLD and the pre-S1 domain are indicated in black. Salt bridges, π interactions, and H-bonds between amino acid side chains along the gating pathway from D388 to K710 are marked in purple, green, and orange, respectively. The minimum hairpin topological loop sizes required to control the relevant non-covalent interactions

are labeled in black. The total numbers of all hairpin loop sizes and non-covalent interactions along the gating pathway are shown in the blue and black circles, respectively.

Figure 5. **The hairpin topological structures along the gating pathway of PI-bound rTRPV1 in the closed state at 4°C and 48°C. A,** Pairing amino acids side chains for salt bridges or H-bonds or cation/CH/π-π interactions along the gating pathway from D388 to K710. The cryo-EM structure of closed rTRPV1 with PI bound at 48°C (PDB ID, 7LPC) was used for the model.[14] The residues are colored in red for a positive charge or blue for a negative charge or orange for the uncharged residues in salt bridges or H-bonds or cation/CH/π-π interactions, and slight green for π interactions. The PI site and the largest hairpin with a 17-residue loop in the interfaces of the VSLD with the TRP domain and the pre-S1 domain are shown in the right panel. **B**, The hairpin topological loop map of closed rTRPV1 at 4°C and 48°C (PDB ID, 7LP9 and 7LPC, respectively). The pore domain, the S4-S5 linker, the TRP domain, the VSLD and the pre-S1 domain are indicated in black. Salt bridges, π interactions, and H-bonds between amino acid side chains along the gating pathway from D388 to K710 are marked in purple, green, and orange, respectively. The minimum hairpin topological loop sizes required to control the relevant non-covalent interactions are labeled in black. The total numbers of all hairpin loop sizes and non-covalent interactions along the gating pathway are shown in the blue and black circles, respectively.

Figure 6. The tentative model for the heat-dependent hairpin melting for thermo-gated TRPV1 opening and desensitization. A. The cryo-EM structures of rTRPV1 in the closed and open and desensitized states (PDB ID: 7LPB, 7LPE, 7LPD, respectively) were used for the model.[14] In the absence of PI at the capsaicin site, rTRPV1 is closed above 25°C but below the threshold 42°C and has the largest hairpin with a 21-residue loop in the interfaces of the VSLD with the TRP domain and the pre-S1 domain. When the temperature increases above the threshold 42^0C, rTRPV1 is open upon the decrease of the largest hairpin size from 21 to 13 residues in the loops, and the total numbers of all non-covalent interactions and hairpin sizes along the gating pathway from D388 to K710 also decrease from 53 and 131 to 44 and 85, respectively. However, in the desensitized state, rTRPV1 further inactivates with the decrease of the largest hairpin size and the total hairpin sizes along the gating pathway from 13 and 85 to 10 and 68 residues, respectively. Of note, the total number of non-covalent interactions is still around 45 along the gating pathway

in the open and desensitized states. **B.** The proposed smaller gating hairpins for heat-activated opening of rTRPV1. The hairpin loop sizes are shown in the red circles.

Figures

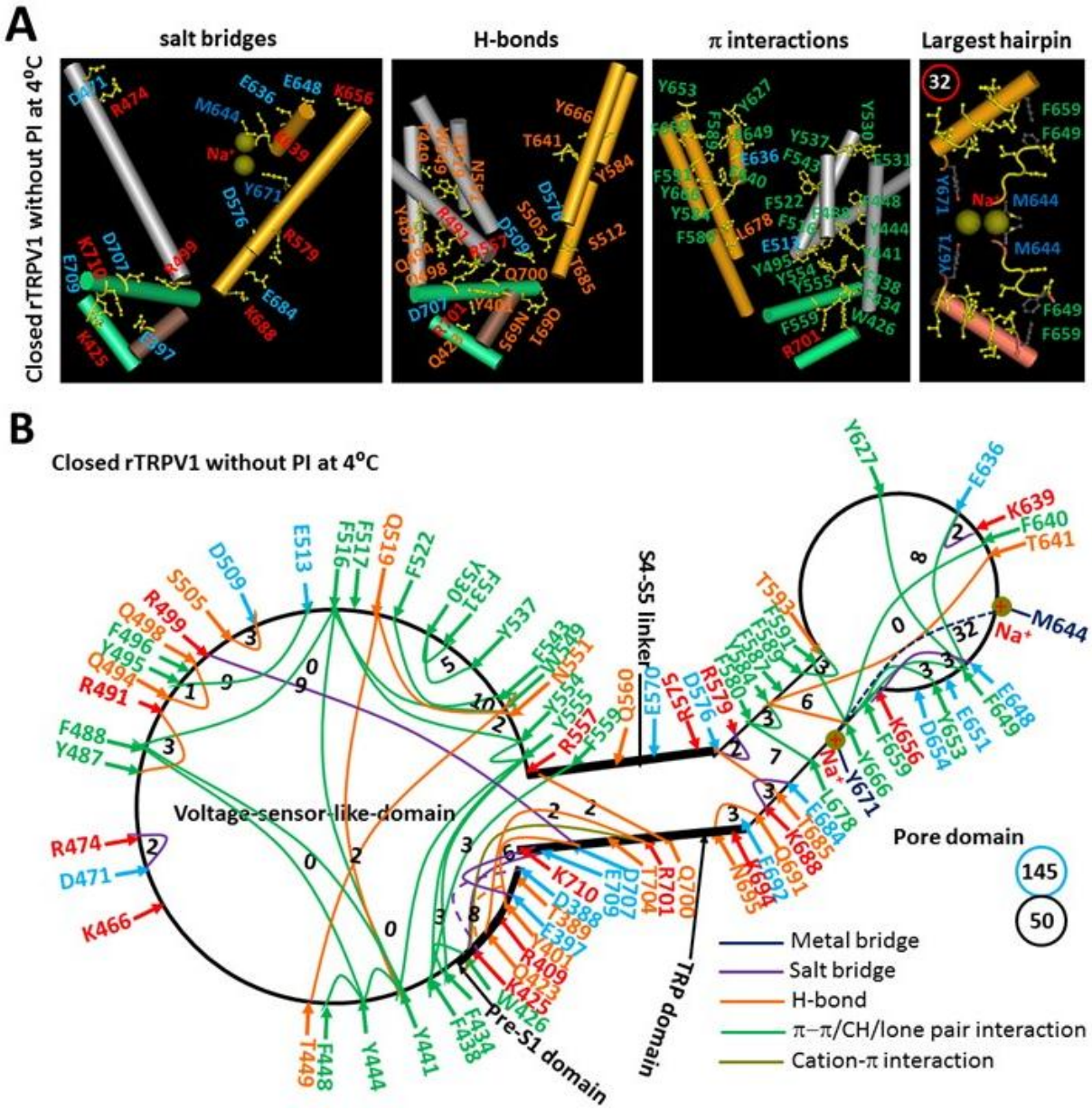

Figure 1

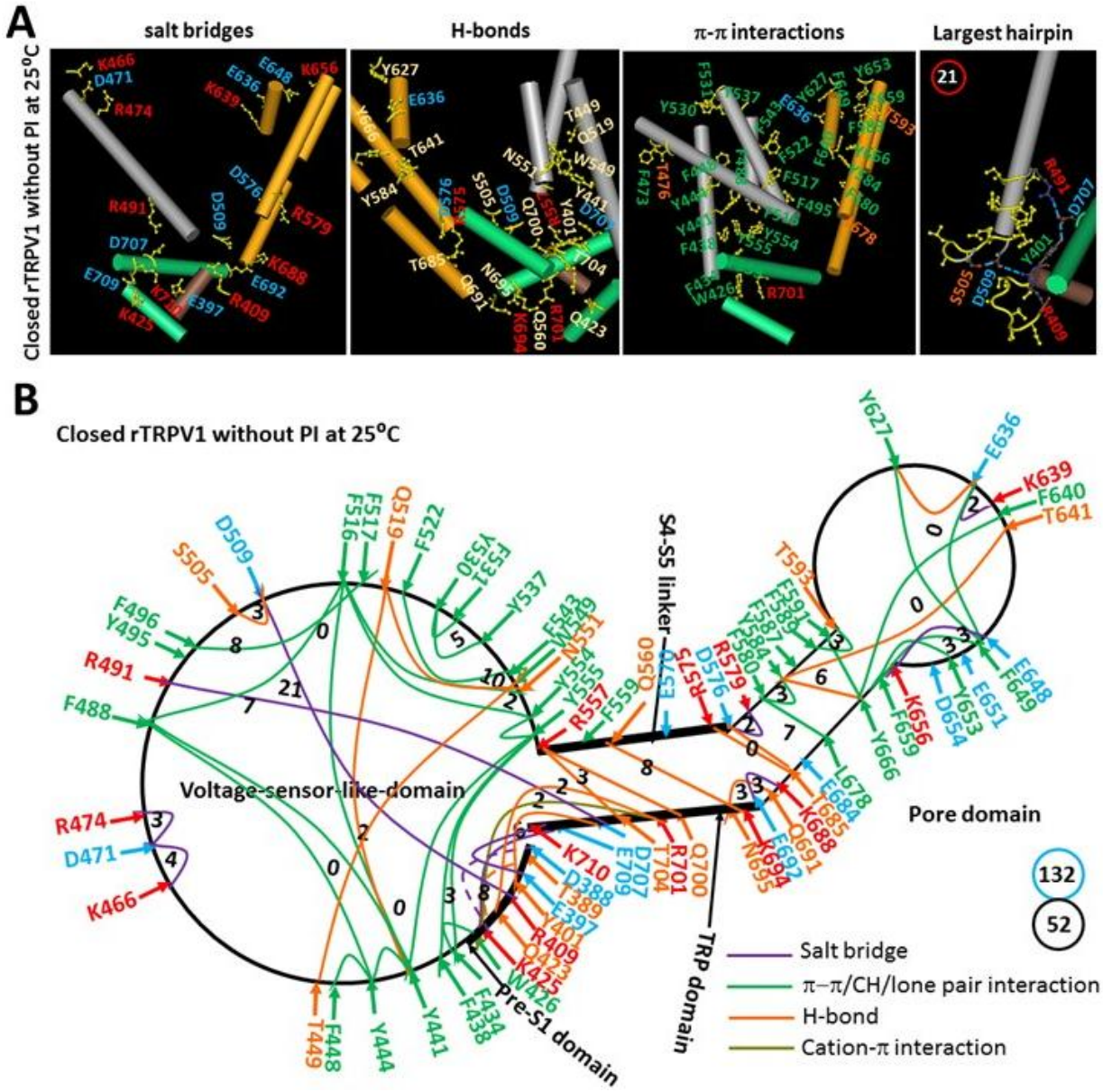
A
salt bridges
H-bonds
π-π interactions
Largest hairpin
Closed rTRPV1 without PI at 25°C
B
Closed rTRPV1 without PI at 25°C
Voltage-sensor-like-domain
Pore domain
S4-S5 linker
Pre-S1 domain
TRP domain
132
52
Salt bridge
π−π/CH/lone pair interaction
H-bond
Cation-π interaction

Figure 2

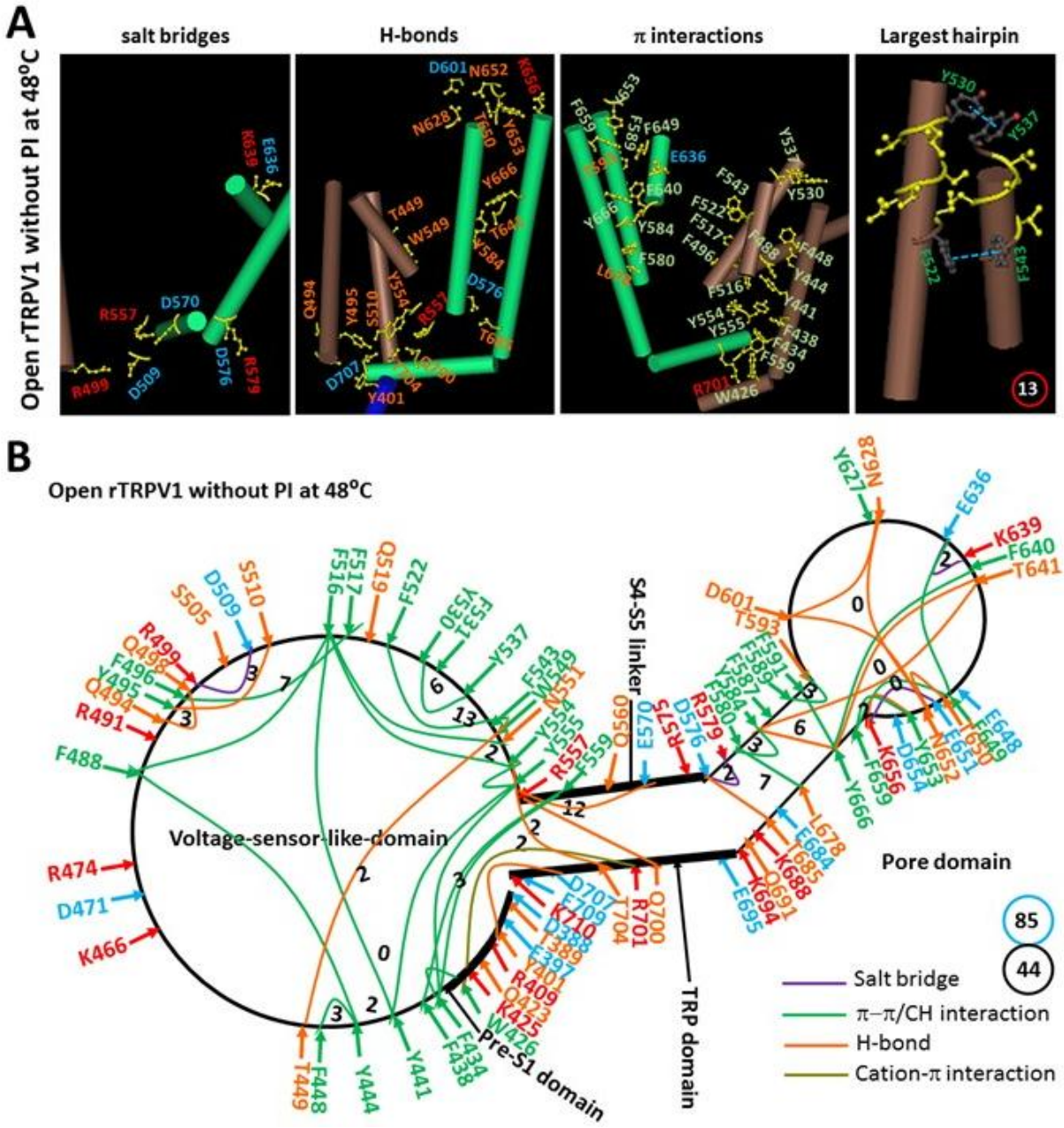
A
Open rTRPV1 without PI at 48°C
salt bridges
H-bonds
π interactions
Largest hairpin
13
B
Open rTRPV1 without PI at 48°C
Voltage-sensor-like-domain
Pore domain
S4-S5 linker
Pre-S1 domain
TRP domain
85
44
Salt bridge
π−π/CH interaction
H-bond
Cation-π interaction

Figure 3

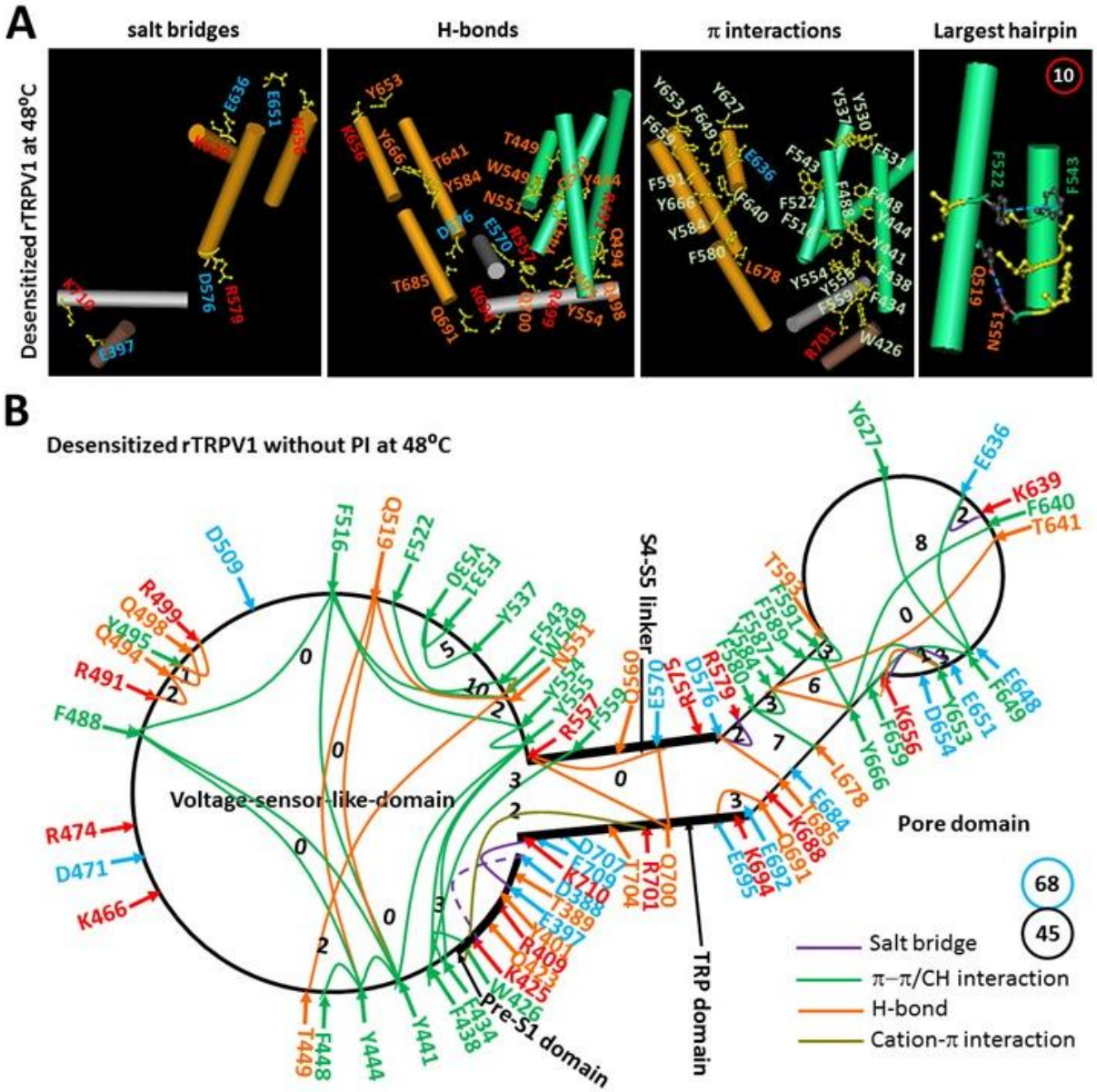
A
salt bridges
H-bonds
π interactions
Largest hairpin
Desensitized rTRPV1 at 48°C
B
Desensitized rTRPV1 without PI at 48°C
Voltage-sensor-like-domain
Pore domain
S4-S5 linker
Pre-S1 domain
TRP domain
Salt bridge
π−π/CH interaction
H-bond
Cation-π interaction

Figure 4

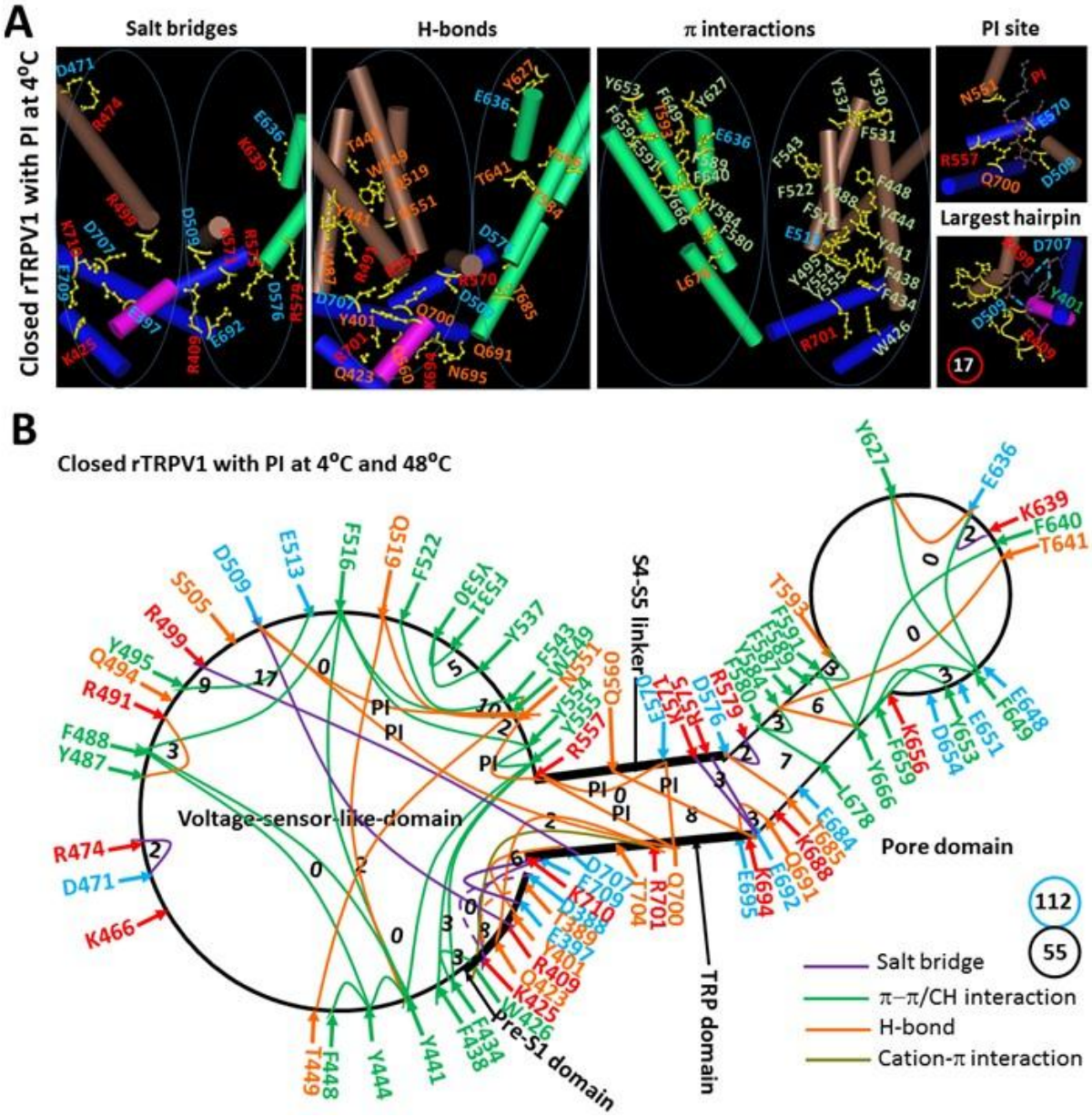
A
Salt bridges
H-bonds
π interactions
PI site
Closed rTRPV1 with PI at 4°C
Largest hairpin
17
B
Closed rTRPV1 with PI at 4°C and 48°C
S4-S5 linker
Voltage-sensor-like-domain
Pore domain
Pre-S1 domain
TRP domain
112
55
Salt bridge
π−π/CH interaction
H-bond
Cation-π interaction

Figure 5

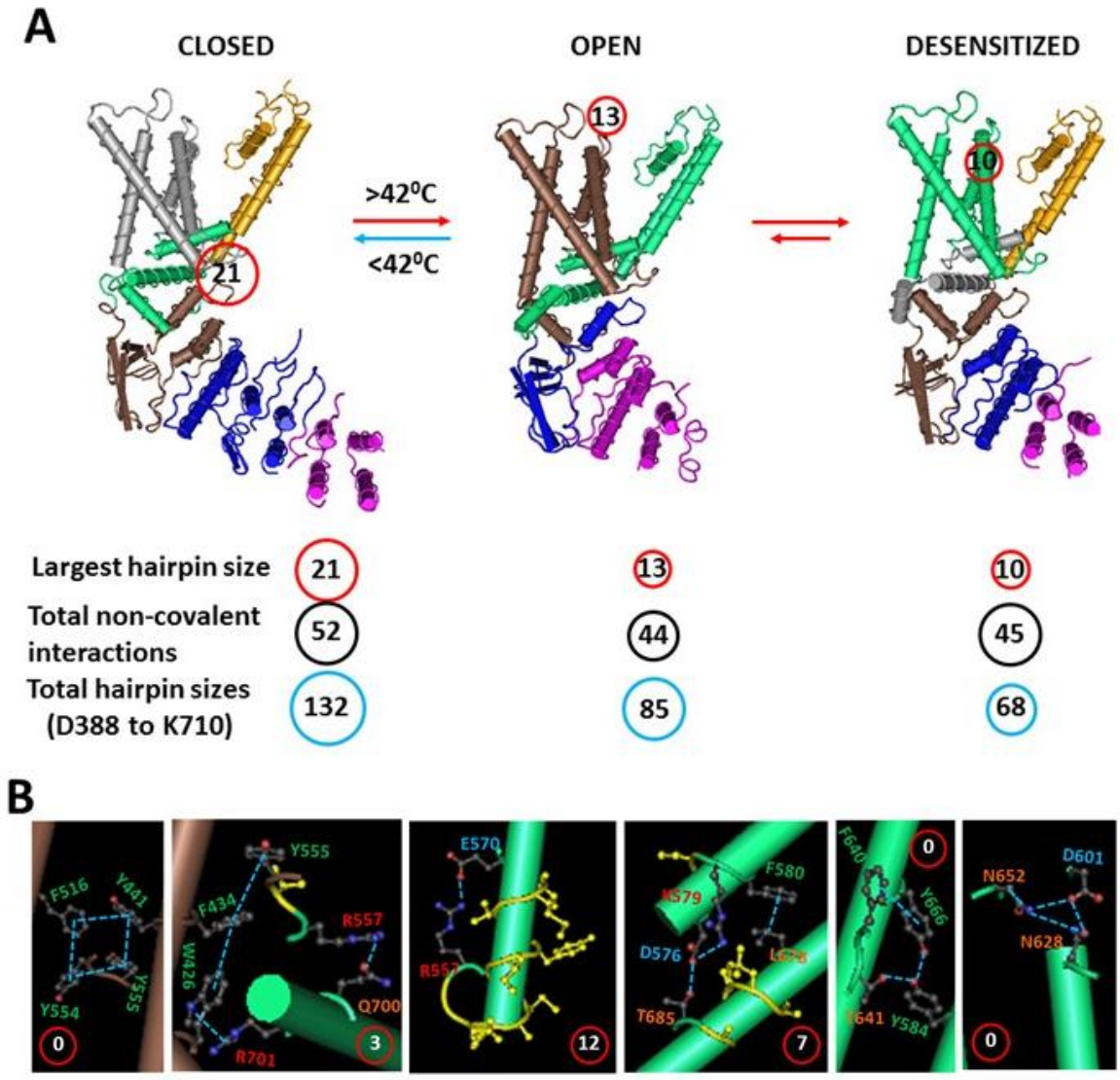
A
CLOSED
OPEN
DESENSITIZED
>42⁰C
<42⁰C
21
13
10
Largest hairpin size
21
13
10
Total non-covalent interactions
52
44
45
Total hairpin sizes (D388 to K710)
132
85
68
B
F516
Y441
Y554
Y555
0
Y555
F434
R557
W426
Q700
R701
3
E570
R557
12
F580
K579
D576
L578
T685
7
F640
0
Y666
T641
Y584
D601
N652
N628
0

Figure 6